The Geology of Pluto and Charon Through the Eyes of New Horizons

J. M. Moore[1]*, W. B. McKinnon[2], J. R. Spencer[3], A. D. Howard[4], P. M. Schenk[5], R. A. Beyer[6,1], F. Nimmo[7], K. N. Singer[3], O. M. Umurhan[1], O. L. White[1], S. A. Stern[3], K. Ennico[1], C. B. Olkin[3], H. A. Weaver[8], L. A. Young[3], R. P. Binzel[9], M. W. Buie[3], B. J. Buratti[10], A. F. Cheng[8], D. P. Cruikshank[1], W. M. Grundy[11], I. R. Linscott[12], H. J. Reitsema[3], D. C. Reuter[13], M. R. Showalter[6], V.J. Bray[14], C. L. Chavez[1], C. J. A. Howett[3], C. M. Lisse[8], A. H. Parker[3], S. B. Porter[3], S. J. Robbins[3], K. Runyon[8], T. Stryk[15], H. B. Throop[16], C. C. C. Tsang[3], A. J. Verbiscer[17], A. M. Zangari[3], A. L. Chaikin[18], D. E. Wilhelms[19]

[1]National Aeronautics and Space Administration (NASA) Ames Research Center, Space Science Division, Moffett Field, CA 94035, USA.
[2]Department of Earth and Planetary Sciences, Washington University, St. Louis, MO 63130, USA.
[3]Southwest Research Institute, Boulder, CO 80302, USA.
[4]Department of Environmental Sciences, University of Virginia, Charlottesville, VA 22904, USA.
[5]Lunar and Planetary Institute, Houston, TX 77058, USA.
[6]The SETI Institute, Mountain View, CA 94043, USA.
[7]University of California, Santa Cruz, CA 95064, USA.
[8]Johns Hopkins University Applied Physics Laboratory, Laurel, MD 20723, USA.
[9]Massachusetts Institute of Technology, Cambridge, MA 02139, USA.
[10]NASA Jet Propulsion Laboratory, La Cañada Flintridge, CA 91011, USA.
[11]Lowell Observatory, Flagstaff, AZ 86001, USA.
[12]Stanford University, Stanford, CA 94305, USA.
[13]NASA Goddard Space Flight Center, Greenbelt, MD 20771, USA.
[14]University of Arizona, Tucson, AZ 85721, USA.
[15]Roane State Community College, Oak Ridge, TN 37830, USA.
[16] Planetary Science Institute, Tucson, AZ 85719, USA.
[17]Department of Astronomy, University of Virginia, Charlottesville, VA 22904, USA.
[18] Independent Science Writer, Arlington, VT, USA.
[19]U.S. Geological Society, Retired, Menlo Park, CA, USA.

Abstract: NASA's New Horizons spacecraft has revealed the complex geology of Pluto and Charon. Pluto shows ongoing surface geological activity centered on a vast basin containing a thick layer of volatile ices that is involved in convection and advection, with a crater retention age no greater than 10 Ma. Surrounding terrains show active glacial flow, apparent transport and rotation of large buoyant water-ice crustal blocks, and pitting by sublimation erosion and/or collapse. More enigmatic features include tall mounds with central depressions that are conceivably cryovolcanic, and ridges with complex bladed textures. Pluto also has ancient cratered terrains up to 4 Ga old that are extensionally fractured and extensively mantled and eroded by glacial or other processes. Charon is not currently active, but experienced major extensional tectonism and resurfacing (probably cryovolcanic) nearly 4 billion years ago. Impact crater populations on Pluto and Charon are not consistent with the steepest proposed impactor size-frequency distributions.

One Sentence Summary: NASA's New Horizons spacecraft has revealed surprisingly complex geology on the surfaces of Pluto and Charon, with probable ongoing activity on Pluto.

Introduction

We report on the preliminary geological examination of Pluto and Charon based on images and other data collected by NASA's New Horizons spacecraft during its flyby of these worlds on 14 July 2015. The two camera systems pertinent to geology are the wide-angle color Multispectral Visible Imaging Camera (MVIC) and the narrow-angle panchromatic LOng Range Reconnaissance Imager (LORRI) (*1*). This report focuses on the portions of the illuminated surfaces seen near closest approach at better than 1 km resolutions, centered on 180° longitude for Pluto and 0° longitude for Charon (*2*). All feature names used in this report are informal. All topographic measurements come from photoclinometric and/or stereo photogrammetric techniques, supplemented by shadow and limb measurements. See the supplementary online material (SOM) for an acronym list.

Pluto

Pluto's surface exhibits an astonishing variety of landscapes (Fig. 1a). Broadly, the encounter hemisphere (EH) contains several regional provinces: (1) the ~1000 km wide uncratered plain, Sputnik Planum (SP), centered on the EH; (2) arcuate, rugged-to-mountainous regions surrounding SP on three sides; (3) mantled and eroded plains at higher latitudes; and (4) a heterogeneous surface west of SP containing plains with various degrees of crater density and surface texture, scarps (both erosional and tectonic), troughs (graben), and patches of rugged cratered terrain.

Sputnik Planum and environs

This ~870,000 km^2 oval-shaped unit of high-albedo plains, centered at ~20°N, 175°E, is likely a massive unit of volatile ices (solid N_2, CO and CH_4) (*3*) set within a topographic basin of at least 3-4 km relief. The central and northern regions of SP display a distinct cellular pattern (*3*), which varies in appearance across the planum. In the bright central portion (Fig. S7a), the cells are bounded by shallow troughs up to 100 m deep (*3*); the centers of at least some cells are elevated by ~50 m relative to their edges, though some apparently have less relief. The southern region and eastern margin of SP do not display cellular morphology, instead showing featureless plains and dense concentrations of pits, themselves reaching a few kilometers across (Fig. S7d). Details of the different morphologies encountered within SP are described in the SOM.

No impact craters have been confirmed on SP in contiguous mapping coverage at 390 m/pixel scale. Following the arguments in (*3*), the crater retention age of SP is very young, and is discussed in SOM. Such geologically recent resurfacing and/or topographic relaxation is consistent with the weak rheologies of N_2 and CO ices (*4, 5*), and with the interpretation of potentially active cells as expressions of solid-state convection in a thick layer of such ices (SOM).

A discontinuous chain of mountains, consisting of discrete angular blocks with apparently random orientations and sizes up to 40 km across and 5 km high, extends for hundreds of km along the west margin of SP. Those in the south are often separated by embaying materials, whereas those in the north, particularly the northernmost al-Idrisi Montes (AIM, Fig. 2), have minimal separation. Here, blocks are closely packed, and many blocks have flat or gently sloping upper surfaces with linear textures similar to some of the surrounding highland terrain, indicating breakup of a preexisting surface.

The northern inter-block material has a distinctive reddish color, contains many smaller blocks, and is slightly elevated relative to SP; similar terrain surrounds some of the mountains to the south. The AIM region contains two depressions floored largely by this finer, inter-block material and small blocks (C), and another occupied by a small plain with similar texture and color to SP (E). An inward-facing terrace surrounds this depression (D), suggesting an earlier, higher level of plains material.

In (*3*) it was argued that the steep slopes and high elevations of the mountain blocks require a water-ice-based composition; this has now been confirmed in LEISA spectra (*6*). Like the angular blocks in europan chaos, Pluto's mountain blocks appear to consist of fragments of pre-existing ice crust that have been detached by fracturing, transported, and rotated (SOM). The exclusive location of this chaotic, blocky mountainous terrain on the margins of SP (Fig. S19), which evidently contains a significant thickness of low-viscosity ices, makes it plausible that these ices play a role in the disruption of Pluto's crust.

Water ice is buoyant with respect to N_2 and CO ice, and blocks of water ice embedded or buried in solid N_2 (and/or CO) will seek to rise isostatically. Small blocks can be carried along by convective or advective motions, essentially as icebergs, and large blocks may be undermined, shifted, and rotated. Even the largest mountains on Pluto could be floating if the solid N_2/CO ice is sufficiently deep (SOM). Melting of N_2 or CO ice at depth in SP could in addition create a fluid that could undermine or "quarry" water ice blocks. Why mountainous terrains within SP are limited to its western margin is unknown.

Pits, blades, plains, and glaciers east of SP

An intricate, high-albedo, 500 km wide landscape of pitted uplands and smooth plains, bordered by lower albedo bladed terrain, forms most of the eastern portion of Tombaugh Regio (TR).

Pitted uplands: The dominant features are pits (Fig. 3a), most of which are a few km across, but some exceed 25 km, locally intersecting to form long, linear troughs. Based upon preliminary topography, pits average ~1 km deep. The crests of the pits define an undulating upland surface 2 to 4 km above SP. In parts of the uplands the pitting is organized into distinct NE-SW trending ridge-and-trough terrain with ~5 km crest-to-crest spacing. The sidewalls of the pits typically slope up to 30º, suggesting rigid material underlies the thin, bright surface layer.

Bladed terrain: The pitted uplands transition northeastward to several broad (~100 km wide) swells named Tartarus Dorsa (TD), whose flanks and crests are covered with numerous roughly aligned blade-like ridges oriented ~N-S (Fig. 3b). Individual ridges are typically several hundred meters high, and are spaced 5 to 10 km crest to crest, separated by V-shaped valleys with slopes of ~20°. Many ridges merge at acute angles to form Y-shape junctions in plan view. Along the west flank of TD are a number of triangular to rectangular facets of the rolling plains ramping upward toward the east.

Smooth plains: Nearly level expanses of smooth plains up to 50 km across occur at relative low points in the pitted uplands as well as elevated terraces adjacent to SP (Fig. 3a). They are generally smooth at 300 m/pixel resolution, but locally collections of km-scale hills extend above the plains, probably as protrusions or embedded fragments of the pitted terrain material. The smoothness of the level plains suggests that they are composed of deformable ices, probably similar in composition to SP.

Glaciers: At a few locations along the SP/uplands boundary, smooth materials connect with SP along the floors of troughs 1.5 to 6 km wide (Fig. 3a). High-phase imaging of the southernmost of these systems reveals conspicuous medial flow lines within the troughs extending onto SP, with the ice in the troughs sloping 2-3º over more than 50 km (SOM). This pattern implies glacial-like flow of the plains material into SP, perhaps analogous to ice streams at the margins of terrestrial ice sheets. At present it is unresolved whether the flowing ice carved the troughs.

Origin and Evolution of Pitted Uplands, Bladed Terrain and Smooth Plains: Pitted and bladed terrains may be remnants of a formerly continuous deposit degraded either by sublimation (forming features analogous to those of degraded terrestrial snow or ice fields - penitentes and sun-cups - but much larger), or through undermining and collapse, possibly through melting at depth. A third possibility is growth of ridges through preferential deposition of volatiles on ridge crests, analogous to pinnacle formation on Callisto (*7*). The preferential orientation of troughs and ridges suggests an origin influenced by solar illumination direction and/or atmospheric circulation. If the bladed-terrain-forming material was exposed through upwarping and erosion, it must have been a once-buried layer. The high albedo of east TR (Fig. 1a) suggests condensation of volatiles sublimated and transported from SP; these may accumulate to form the smooth plains.

Upland terrains: Washboard, dissected, and fretted terrains and eroded mantles

The uplands north and northwest of SP contain a variety of morphologies, notably including expanses of parallel ridges and troughs we call washboard terrain, and dissected terrain locally organized into dendritic valley networks.

Washboard terrain: Many flat expanses in this region feature parallel ridges and grooves with a crest-to-crest wavelength of about 1 km (Fig. 4a). The ridges retain a consistent NE-SW orientation, even where developed on the interior floors of craters. The albedo of washboard surfaces matches that of nearby ungrooved terrain, and underlying terrain features remain visible where grooved. These observations suggest that washboarding is a superficial modification, either by erosion of the underlying surface or, alternatively, as part of a thin regional deposit. The grooving is superimposed on higher-relief topographic features such as ridges, craters and dissected terrain. Occasional 1-2 km diameter craters are superposed on the washboarding.

Dissected terrain: Terrains dissected by valleys are common on the EH, including fluted, valley network, plateau, alpine and mountainous variants (Fig. 4b). Two of these types occur widely. *Fluted slopes* of troughs 15-20 km across with up to 2 km relative relief that are eroded into broad hills constitute one of these. The troughs or flutes are regularly spaced at 3-4 km and are oriented down-gradient with slopes up to 20°. The interior walls of some craters are similarly fluted. These troughs terminate abruptly in depressions or crater floors without evidence of deposition. Similarly spaced *dendritic valley networks* are another type of dissected terrain. The networks generally terminate in broad depressions. Both dissected terrain and valley networks appear to post-date and modify the larger upland craters. The other styles of dissection are described in SOM.

Fretted terrain: Northwest of Burney crater (Fig. S8), fretted terrain consists of bright plains cut into polygons by a network of darker troughs 3 to 4 km wide. Numerous craters (<25 km diameter) occur within this terrain, some with dark floors.

Eroded mantles: Various eroded mantles characterize the high northern latitudes commencing about 200 km away from SP and continuing to the limb from NE to NW. The

density of craters is low except for a few degraded examples ~50 km across. The mantles range from rough-surfaced with steep marginal scarps to smooth with convex rounded edges. The steep scarps are likely erosional, but the convex scarps may be depositional. Locally the surfaces have been eroded by steep-sided pitting that reaches 3-4 km deep (Fig. S9). To the NW the mantles are interspersed with expanses of plains. Some of the scarps appear similar to the dissected terrain described above. The mantles in the NE and NW sectors have a bluish tint whereas the rough mantles surrounding the pole have a distinct yellowish appearance with parallel lineations and troughs crossing the pole (Fig. 1a). The mantles are in excess of 1 km thick in places.

Origins of these terrains: The mechanisms regulating the characteristic scale and groove orientation of washboarding remain uncertain. Both the fluted slopes and the valley networks probably result from advective processes, most likely flow of nitrogen-rich ice, possibly accompanied by basal melting. The fretted terrain may likewise be shaped by glaciation or may involve differential sublimation. The eroded mantles may have been modified by flow. Further discussion of these possibilities is contained in the SOM.

Western low latitude terrains

Here we discuss the several terrains west of Sputnik Planum, including the large, low albedo feature Cthulhu Regio (CR), and the region to its north.

Smooth Plains: An extensive, low-elevation, mottled plain occurs at the western end of Innana Fossa, bounded by an arcuate scarp along its southern and western borders (Fig. S10). It has a much lower crater density than surrounding regions. Despite the younger fracture system, it is significantly smoother than intercrater plains in adjacent areas. Scarp retreat appears to have been active in this region.

Bright-halo craters: In the region north of CR, centered on 25°N, 125°E, craters feature dark floors and bright rims and outer flanks, in contrast to craters elsewhere. Even within this subset of craters (Fig. S11), there is variation in their colors and albedos, including between north- and south-facing slopes within the same crater.

Cthulhu Regio: CR is a large dark area that covers a swath from the equator to ~20°S (Fig. S20), bordering TR at 160°E, and stretching westward almost half way around the planet to 20°E. Eastern CR is not a distinct physiographic province, but instead a region of dark mantling thin enough to preserve underlying topography, superimposed upon various geological terrains, including dendritic valleys, craters, fossae, and retreating scarps. The dark coating is likely the result of atmospheric tholin deposition (*6*). CR contains striking correlations between color/albedo and topography: bright material is correlated with high elevations in some areas and with north-facing slopes in others. This may result in part from insolation-dependent deposition of either dark or bright material.

Large mounds with central depressions

To the southwest of Norgay Montes are two broad quasi-circular mounds (Fig. 5). The northernmost (Wright Mons, WM) is 3-4 km-high and ~150 km across. At its summit is a 5-km-deep central depression that has a rim showing concentric fabric. The mound surface has a hummocky/blocky surface texture, and is very lightly cratered. A similar but even larger feature (Piccard Mons, PM) is seen in twilight stereo imaging 300 km to the south. This reaches ~6 km high and 225 km across. The general shapes of these edifices and associated structures appear to be constructional. Their origin could involve cryovolcanism.

Tectonics

Pluto's EH shows abundant extensional features in varying stages of degradation. Notable is the single 3-4-km deep V-shaped trough, Virgil Fossa (VF, Fig. S12c), which extends unbroken for at least 200 km and has an asymmetric upward displacement on the south flank of 1-2 km. Towards the trough's eastern end it cuts through Elliot crater, and to the west links with a network of smaller subparallel fractures. The scarp has an anomalously red color, perhaps indicating recent exposure, and is associated with water ice (*6*). Other extensional fracture systems are shown in Fig. S12.

Compressional features are less obvious. One candidate, TD (Fig. S12f), consists of several elongated swells ~200 km wide, traversed by at least one long extensional feature (Sleipnir Fossa, SF). TD could be due to compressional folding, but also resembles diapiric upwellings, perhaps including extrusion onto the surface (e.g. salt domes or walls; *8*).

The differing fault trends and states of degradation suggest multiple deformation episodes and prolonged tectonic activity. The equatorial normal faults would not arise from spin-down stresses or orbital recession (*9*). The great length of individual faults, their steepness, and the absence of flank uplift suggest a thick H_2O-ice lithosphere.

Impact craters

Pluto displays a wide variety of crater sizes and morphologies (Fig. S13). Globally, recognizable crater diameters range from ~0.5–250 km, not including any possible ancient basin underlying SP. Crater densities vary widely on Pluto, from the heavily cratered portions of CR, to SP, which has no identifiable impact craters. The total cumulative crater size-frequency distribution (SFD) on the EH is shown in Fig. S15a. From this we conclude that Pluto's surface as a whole dates

back nearly to the time of the end of Late Heavy Bombardment (LHB), or in the context of the Kuiper belt, the proposed era of rearrangement of the outer solar system (e.g., *10*). On the EH, only the eastern portion of CR appears to approach the saturation crater densities (for large craters, Fig. S15b) that would be expected of a terrain that survived from the LHB itself, when cratering rates were likely much higher than at present. In contrast, TD, eastern TR, the water-ice mountain ranges, the mounds (all very lightly cratered), and especially SP (no identified craters) are very young (Fig. S15c). No craters have been detected in SP down to 2-km diameter, which is a tighter size limit than reported previously (*3*), and implies a model crater retention age of no greater than 10 Ma, and possibly much less (*11*) (SOM).

Geologic evolution

Though complex and largely novel, landforms on Pluto present many clues to their origin and history. The basin in which SP is located is ancient, despite the youthfulness of its interior deposits. Its semicircular rim of elevated mountainous terrains suggests that it probably is a heavily modified impact basin. The larger visible craters in these mountainous terrains probably post-date this likely SP basin.

Except in the west, the uplands surrounding SP have been blanketed with mantles of substantial thickness and various surface compositions (*6*), which have been partially stripped. The primary agents of upland modification probably include sublimation, frost deposition, and glacial erosion. We envision two end-member scenarios: in one, a formerly deep ice mantle (largely N_2) covered the uplands surrounding SP but was gradually lost to space. As ice levels dropped, glacial ice eroded the dissected terrains and, to the east of SP, flowed back into SP, leaving remnants in smooth-floored depressions. Alternatively, ices may have been cycled

between SP and its surroundings, perhaps episodically, to form the glaciers and dissected terrains. In this case loss to space of volatile ices need not have occurred (*12*). Nitrogen and other volatiles available to the surface environment may also be replenished episodically by sources within Pluto's interior (*13*).

The dark mantles of CR and other local regions conform to present topography, suggesting that they post-date the erosional sculpting of the landscape or are actively recycled. The cellular pattern imposed on SP ices is a relatively young feature, given the absence of craters, and the hectometer-scale pits and ridges on SP comprise the youngest widespread landforms on Pluto.

The relative youth of some extensional features is consistent with predicted changes in global stress associated with a late, possibly partial freezing of a subsurface ocean (*14*). Various lines of evidence, including the spectroscopic identification of water ice along the exposed walls of VF, as well as the steep, chaotic mountains bordering SP, suggest a cold, strong, water ice-based crust.

Charon

Charon's EH (Fig. 1b) can be divided into two broad provinces separated by an en echelon assemblage of ridges and canyons, which span the EH from east to west. North of this tectonic belt is rugged, cratered terrain; south of it is smoother but geologically complex plains. The northern hemisphere is capped by the dark, reddish Mordor Macula (MM). Relief exceeding 20 km is seen in limb profiles and stereo topography (Fig. S16), and is testament to the bearing strength of cold water ice and Charon's modest gravity (0.288 m s^{-2}).

Cratered northern terrain

Charon's northern terrain is exceptionally rugged, and contains both a network of polygonal troughs 3-to-6 km deep, and a possibly related irregular depression almost 10 km deep immediately south of the edge of MM near 270°E (Fig. S16). A prominent, ~240-km diameter, 6-km-deep crater (Dorothy Gale) at 58°N, 38°E straddles the discrete edge of MM (*3*). The cumulative crater distribution for Charon's northern terrain is shown in Fig. S17a. The crater density at large sizes, where counts are reliable, implies a surface age older than 4 Gyr (SOM).

The overall dark deposit of MM does not correlate with any specific terrain boundary or geologic unit. A prominent albedo and color boundary to the west in Fig. 1b coincides with a prominent ridge ~5 km high (Fig. S16), which may be an impact basin rim or an extension of the tectonic deformation seen more clearly to the south. Other morphological indicators of an impact origin such as a well-defined ejecta blanket or secondary craters have not been discerned.

Ridges, troughs, and canyons

The structural belt that bisects Charon's EH consists of subparallel scarps, ridges and troughs, of variable extent but over 200 km wide in places (Fig. 1b). Notable are two chasmata: 1) Serenity Chasma is >50 km wide and ~5 km deep, and exhibits a pronounced rift-flank uplift; and 2) Mandjet Chasma, which appears downfaulted, and reaches ~7 km deep. These chasmata resemble extensional rifts on several mid-sized icy satellites (*9*).

We interpret this assemblage as the structural expression of normal faults and graben, that represent substantial, oriented, tectonic extension of Charon's icy crust. Several large craters superposed on the chasmata indicate that this extension is geologically old. Given the horizontal and vertical scale of these structures, steeply dipping normal faults likely extend to depths of tens

of km. They represent extension on the order of ~1%. Argo Chasma, viewed very obliquely along the horizon (*3*), is seen in lower resolution images to have an arcuate planform (Fig. S18), and so could be related to an impact basin, or alternatively, could be a continuation of the fracture/trough system.

Southern Plains

The smoother southern half of Charon's EH forms an apparently continuous surface with low relief named Vulcan Planum (VP). Near the bounding scarps to the north, the planum slopes gently downward by ~1 km towards the scarps. Portions of the plains observed at higher resolution exhibit a distinctive, lineated texture of closely spaced grooves or furrows (Fig. 6). One possible origin is tectonic resurfacing like that seen on the icy satellites Ganymede and Enceladus (*7*). Morphologically distinct groups of deeper, rille-like narrow troughs and furrows that post-date the plains also occur. Although deep, these troughs are nonetheless superimposed by a number of impact craters, and thus are relatively old. The en echelon nature of these troughs, and rough parallelism with the chasmata to the north, suggests a tectonic origin or structural control.

Fields of small hills (2-3 km across), areas of relatively low crater density, and at least one pancake-shaped unit are consistent with cryovolcanic resurfacing (Fig. S6b) (*15*). Peaks surrounded by moat-like depressions (Kubrick and Clarke Montes) were noted by (*3*). The peaks are up to 3-4 km high and the depressions 1-2 km deep. Two additional depressions are surrounded by rounded or lobate margins (Fig. S6a). The depression at Clarke Mons appears to expose a more rugged terrain, with smooth plains embaying the margins, two of which are lobate. The "moats" may be due to mountain loading and flexure of Charon's lithosphere;

alternatively, the moats *and* depressions may be the expressions of the flow of, and incomplete enclosure by, viscous, cryovolcanic materials, such as proposed at Ariel and Miranda (*16, 7*).

The SFD of impact craters of the southern plains lies below that of the north at large diameters (Fig. S17a), yet model ages for the plains point to an age of ~4 Gyr (SOM). In limited regions, however, craters are sparse (Fig. S6b), implying that the resurfacing of VP may have acted over an extended time.

Geological evolution

Charon's surface is dominated by impacts, tectonic deformation, and resurfacing, and as such fits broadly into the paradigm of geologic evolution on icy satellites. That Charon is so geologically complex, however, would seem to require a heat source for reshaping what would have otherwise been a heavily cratered surface. If the 4 Gyr age of even the youngest of Charon's surfaces is correct, then this activity dates back to an early warmer epoch. The tectonic record is consistent with global expansion, and the smooth plains consistent with the mobilization of volatile ices from the interior. The spatial distribution of tectonic features is not readily reconciled with the kinds of patterns expected from tidal or despinning stresses (*7*). Charon may have had an ancient subsurface ocean that subsequently froze, which would generate the global set of extensional features, as well as deep faulting that would permit eruption of cryovolcanic "magmas."

A Divergent Binary

Pluto and Charon are strikingly different in surface appearance, despite their similar densities and presumed bulk compositions (*3*). With the possible exception of MM, the dynamic

remolding of landscapes by volatile transport seen on Pluto is not evident on Charon, whose surface is instead dominated spectrally by the signature of water ice (*6*). Whether this is because Charon's near-surface volatile ices have sublimated and have been totally lost to space owing to that body's lower gravity (*17*), or whether something more fundamental related to the origin of the binary and subsequent internal evolution (*18*) is responsible, remains to be learned.

Much of what we see on Pluto can be attributed to surface-atmosphere interactions and the mobilization of volatile ices by insolation. Other geological activity requires or required internal heating. The convection and advection of volatile ices in SP can be powered by present-day radiogenic heat loss (SOM). On the other hand, the prominent mountains at the western margin of SP, and the strange, multi-km-high mound features to the south are both young geologically (lightly cratered) and presumably composed of relatively strong, water-ice-based geological materials. Their origin, and what drove their formation so late in Solar System history remain uncertain. What is more certain is that all three major Kuiper belt bodies visited by spacecraft so far, Pluto, Charon, and Triton, are more different than similar, and bear witness to the potential diversity awaiting the future exploration of their realm.

Acknowledgements

We thank the many engineers who have contributed to the success of the New Horizons mission and NASA's Deep Space Network for a decade of excellent support to New Horizons. We also thank Pam Engebretson for input regarding production of the figures in this paper. This work was supported by NASA's New Horizons project.

References

1. H.A. Weaver *et al., Space Sci. Rev*. **140,** 75–91 (2008). doi: 10.1007/s11214-008-9376-6

2. L.A. Young *et al., Space Sci. Rev.* **140**, 93-127 (2008). doi: 10.1007/s11214-008-9462-9

3. S.A. Stern *et al., Science* **350**.6258 (2015). doi:10.1126/science.aad1815

4. J. Eluszkiewicz, D.J. Stevenson, *Geophys. Res. Lett.* **17**, 1753–1756 (1990). doi: 10.1029/GL017i010p01753

5. Y. Yamashita *et al.*, *Icarus* **207**, 972-977 (2010). doi: 10.1016/j.icarus.2009.11.032

6. W. Grundy *et al.,* this issue.

7. J.M. Moore *et al*., *Icarus* **246**, 65–81 (2015). doi: 10.1016/j.icarus.2014.04.028

8. P.M. Schenk, M.P.A. Jackson, *Geology* **21**, 299-302 (1993).

9. G.C. Collins *et al.*, in *Planetary Tectonics*, R.A. Schultz, T.R. Watters, Eds. (Cambridge Univ. Press, New York, 2010) pp. 264–350.

10. R. Gomes *et al.*, *Nature* **435**, 466–469 (2005). doi:10.1038/nature03676

11. S. Greenstreet, B. Gladman, W.B. McKinnon, *Icarus*, **258**, 267-288 (2015). doi: 10.1016/j.icarus.2015.05.026

12. R. Gladstone *et al.,* this issue.

13. K.N. Singer, S.A. Stern, *Astrophys. J. Lett.* **808** L50 (2015). doi:10.1088/2041-8205/808/2/L50

14. G. Robuchon, F. Nimmo, *Icarus* **216**(2), 426-439 (2011).

15. P.M. Schenk, J.M. Moore, in *Solar System Ices*, B. Schmitt, C. de Bergh, M. Festou, Eds. (Kluwer Academic, Dordrecht, 1998) pp. 551–578.

16. D.G. Jankowski, S.W. Squyres, *Science* **241**, 1322–1325 (1988).

17. E.L. Schaller, M.E. Brown, *Astrophys. J. Lett.* **659**, L61–L64 (2007).

18. W.B. McKinnon, in *Treatise on Geophysics*, *2nd Ed.*, *vol. 10*, G. Schubert, Ed. (Elsevier, Amsterdam, 2015), pp. 637–651. doi.org/10.1016/B978-0-444-53802-4.00210-4

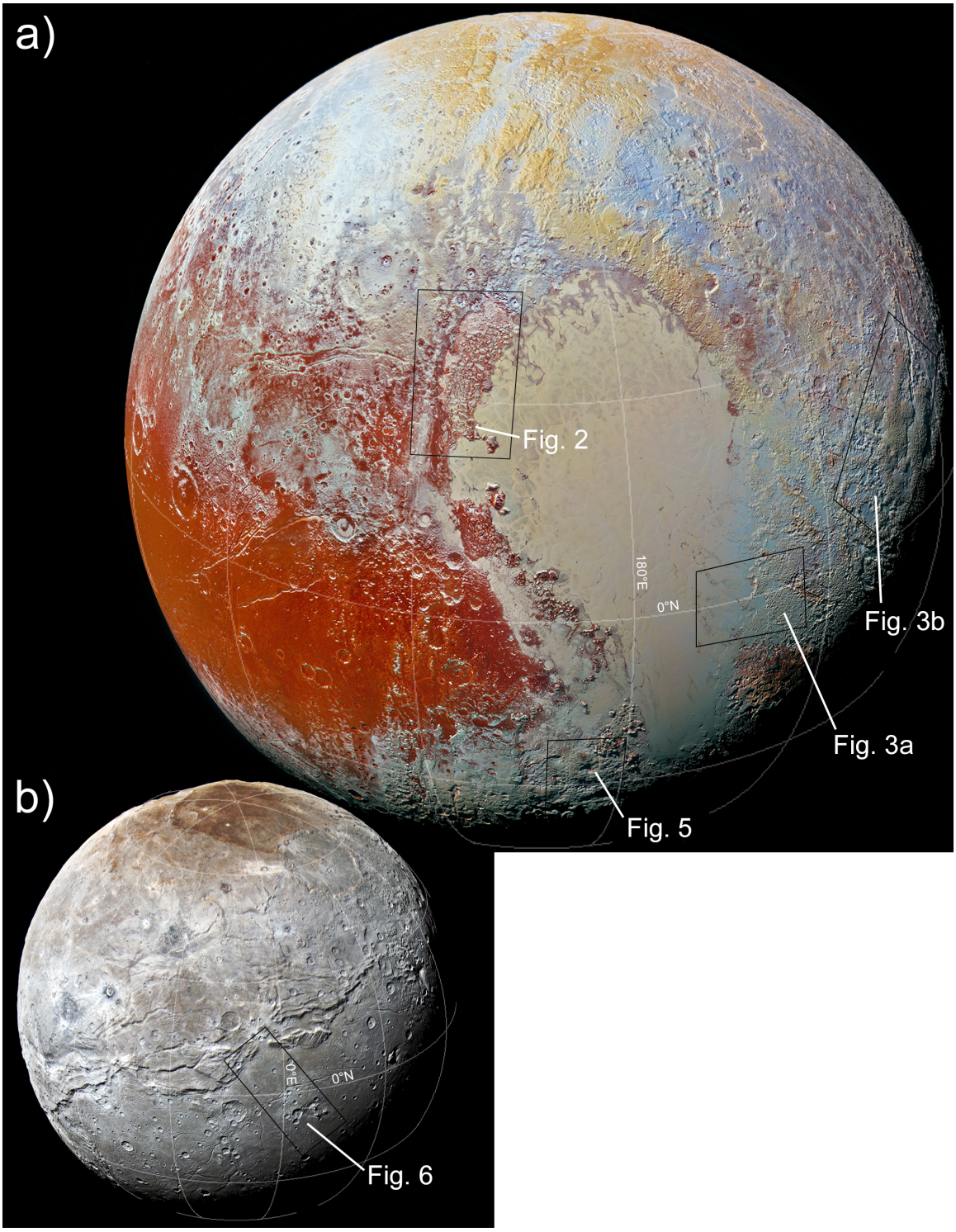

Fig. 1: Global, exaggerated color views of Pluto (a) and Charon (b), with their sizes shown to scale. North is up for both. A number of terrains discussed in the text are highlighted and labeled.

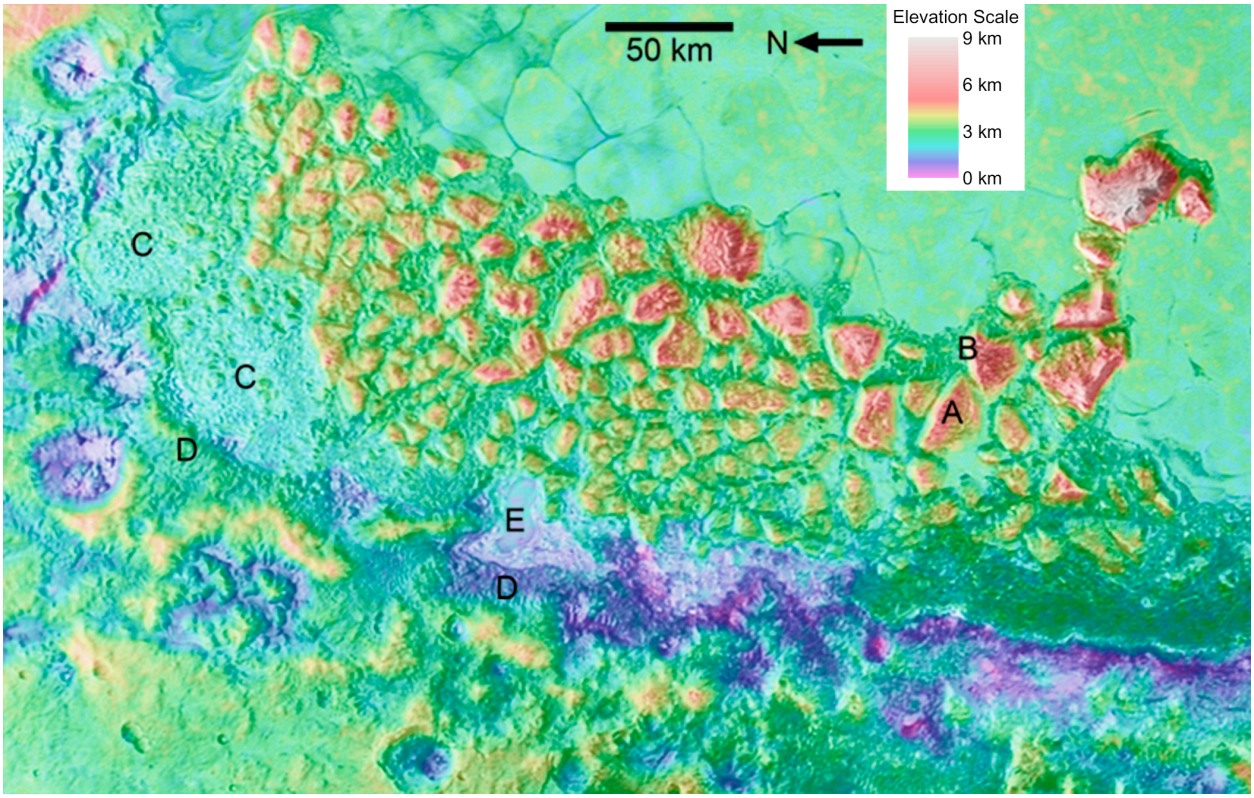

Fig. 2: The chaotic mountains of AIM on the northwest margin of SP. Colorized DEM overlain on MVIC imagery. (A) Textured surface possibly pre-dating block formation; (B) Steep fracture surface with possible exposed layering; (C) Chaos composed of small blocks; (D) Inward-facing terraces; (E) Small exposure of SP-like material.

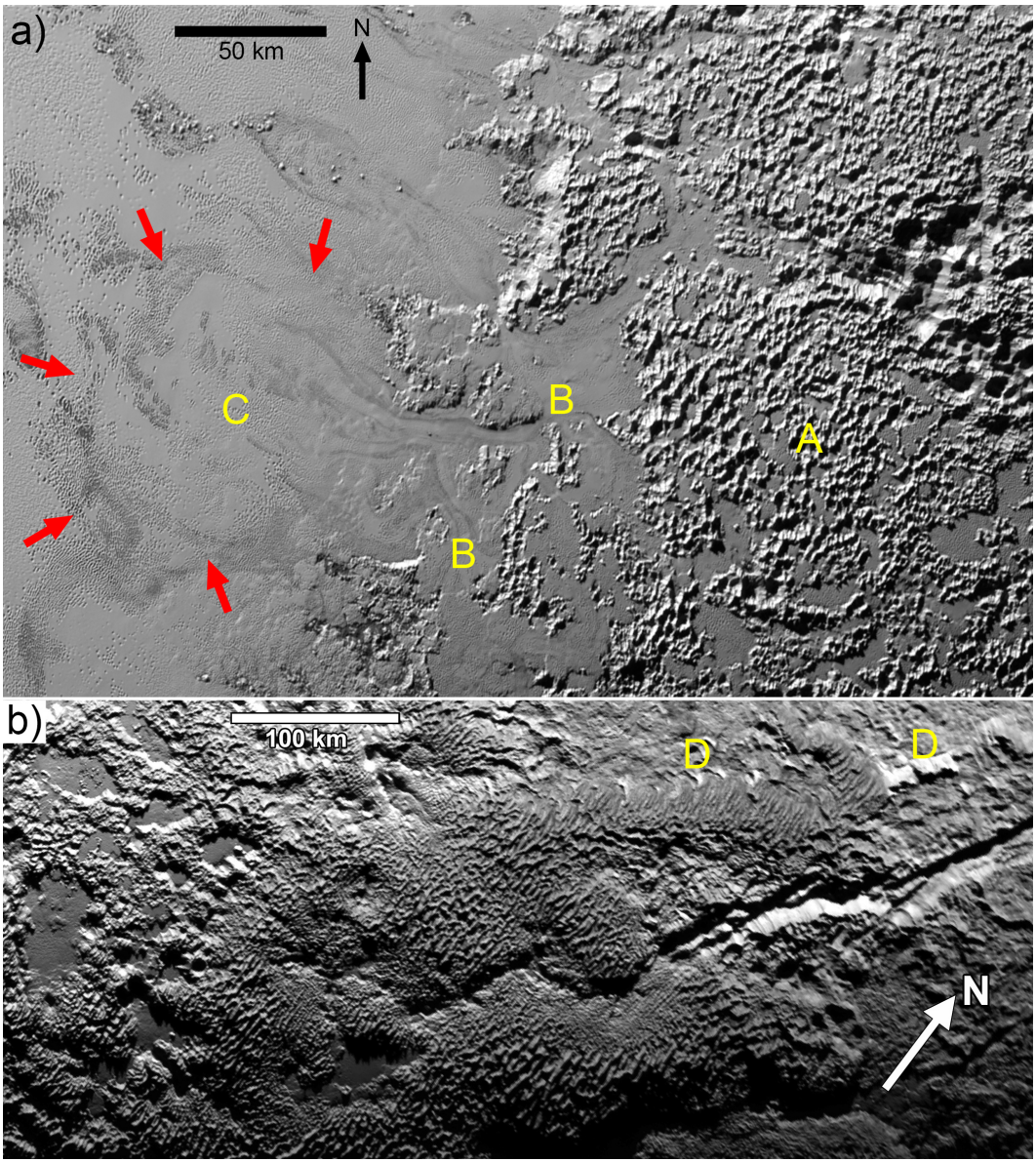

Fig. 3: (a) Pitted uplands and valley glaciers east of SP. (A) Densely pitted terrain, with smooth material covering the floors of the pits. (B) Smooth material exhibiting glacial flow through notches in the pitted uplands towards SP. (C) Debouchment of a valley glacier into SP. Possible outer flow edges are indicated by red arrows.

(b) Aligned ridges outcropping on top of several broad swells of the TD formation. (D) Triangular and rectangular facets of the rolling plains ramping upwards onto the ridges.

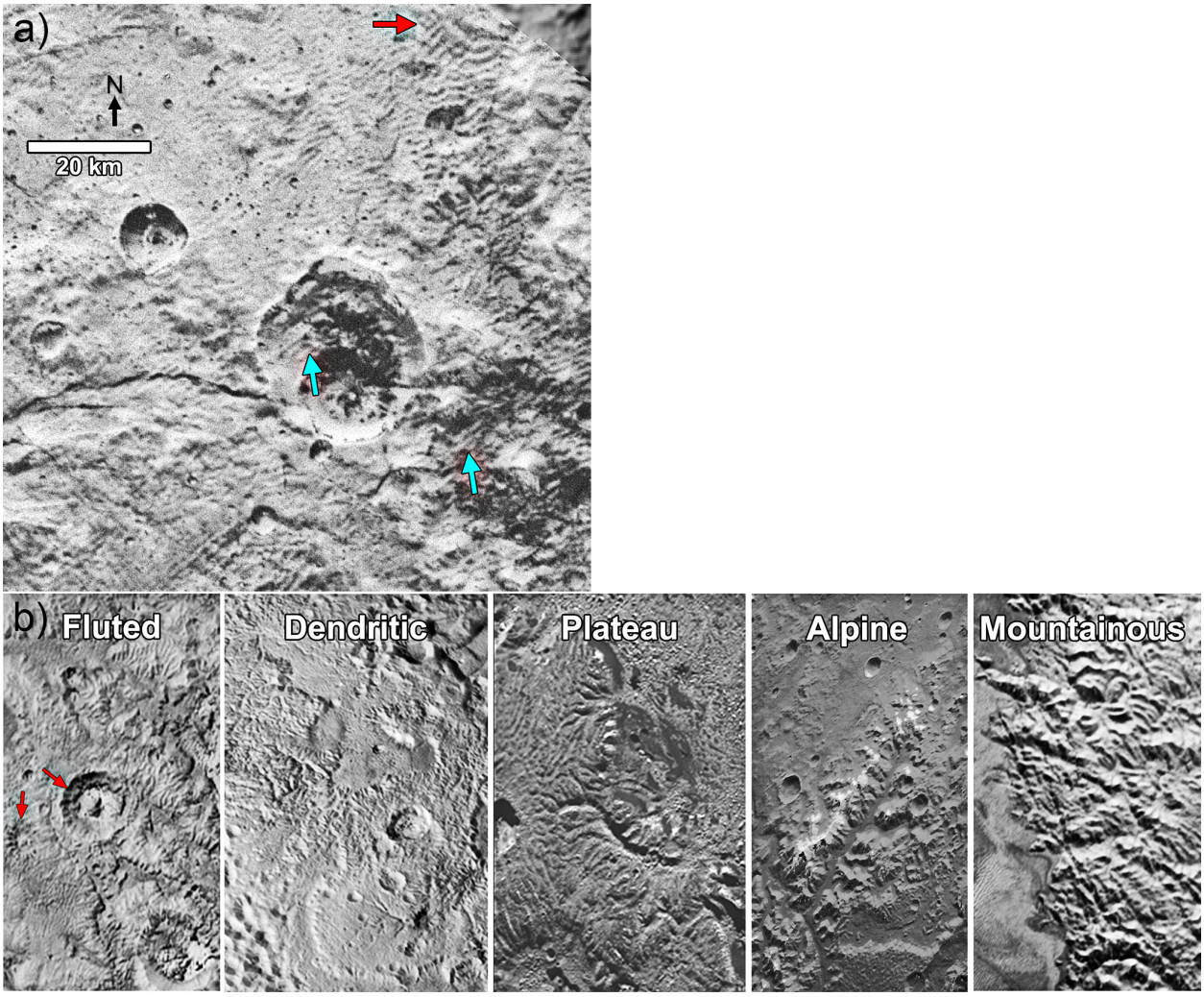

Fig. 4: Washboard and dissected terrains. Locations of the terrains are highlighted in Fig. S4. (a) Washboard terrain northwest of SP. Blue arrows point to washboard texture within craters. Red arrow points to a location where washboard terrain has modified fluted terrain.

(b) The variety of dissected terrains with informal typology discussed in text. Red arrows point to fluting on crater walls. Scales are described in the caption to Fig. S4b.

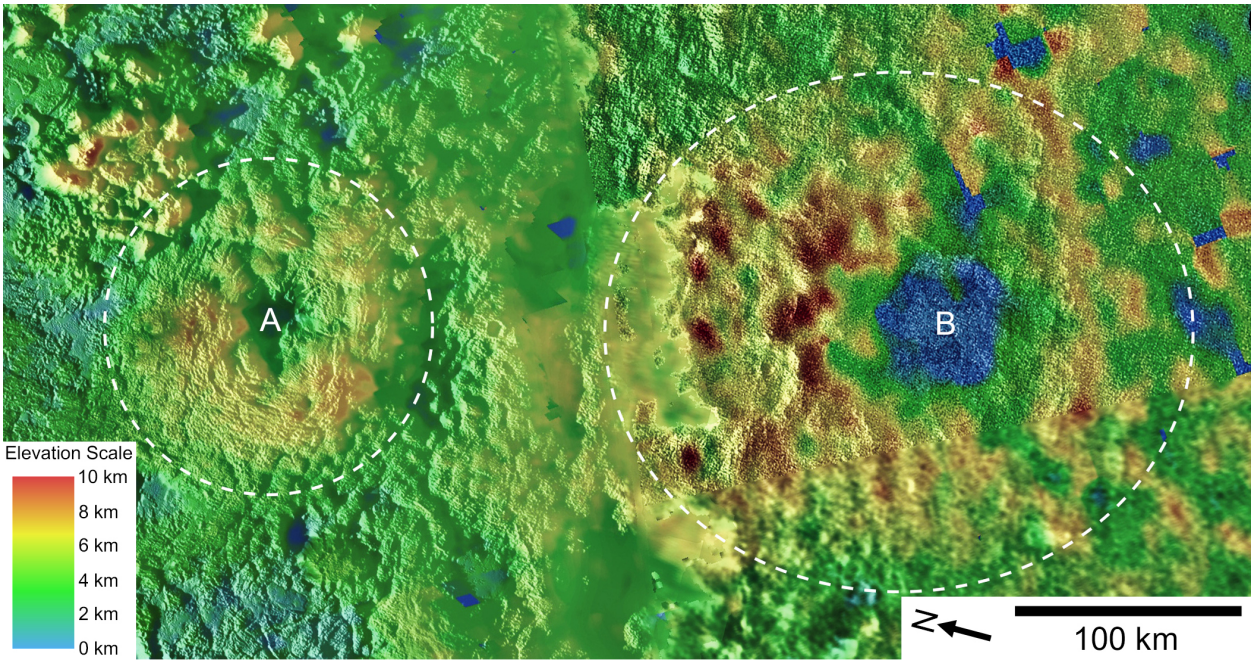

Fig. 5: Quasi-circular mounds south of SP, both with depressions at their summits. Colorized DEM overlain on MVIC coverage of the mounds. Dashed lines mark their approximate boundaries. A marks WM, B marks PM.

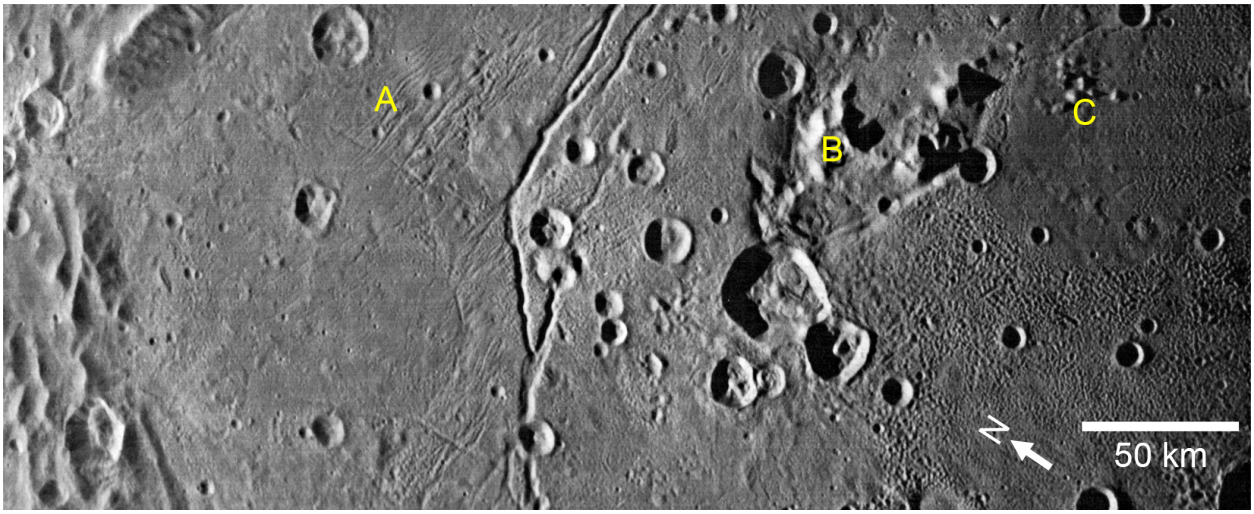

Fig. 6: VP on Charon. (A) Lineated texture in the plains. (B) Clarke Mons. (C) Small hills.